Scripta Materialia 207 (2022) 114274

Contents lists available at ScienceDirect

Scripta Materialia

journal homepage: www.elsevier.com/locate/scriptamat

The effect of deviations from precise [001] tensile direction on creep of Ni-base single crystal superalloys

L. Heep[a,*], D. Bürger[a], C. Bonnekoh[a], P. Wollgramm[a], A. Dlouhy[b], G. Eggeler[a]

[a] Institute for Materials, Ruhr-University Bochum, Bochum 44801, Germany
[b] Institute of Physics of Materials, Academy of Sciences of the Czech Republic, Brno 616 62, Czech Republic

ARTICLE INFO

Article history:
Received 22 April 2021
Revised 3 September 2021
Accepted 6 September 2021
Available online 20 September 2021

Keywords:
Ni-base superalloys
Anisotropy
Creep deformation
Transmission electron microscopy

ABSTRACT

Low temperature (1023 K) high stress (800 MPa) tensile creep behavior of the superalloy single crystal ERBO-1 (CMSX-4 type) is investigated. Three loading directions are compared: precise [001] and 15 ° deviations from [001] towards [111] and [011]. It is found that creep rates $\dot{\varepsilon}$ scale as $\dot{\varepsilon}_{[001]\rightarrow[111]} > \dot{\varepsilon}_{[001]} > \dot{\varepsilon}_{[001]\rightarrow[011]}$ already in the early stages of creep ($\varepsilon \leq 1\%$), where dislocation network formation and planar fault intersections cannot rationalize the observed rate effects. An analysis based on Peach-Köhler force calculations suggests, that fast creep rates are observed, when dislocations from two octahedral systems, which are required to react and form the leading part of a planar fault ribbon in the γ'-phase, experience similar driving forces. Creep data, micromechanical calculations and TEM results are in good qualitative agreement. From a technological point of view, the results show that while 15 ° deviations from [001] towards [011] can be tolerated, deviations towards [111] must be avoided.

Ni-base superalloy single crystals (SXs) are used for blades in gas turbines for aero engines and power plants [1,3]. The blades are cast in a Bridgeman type of process, where the target direction for the longitudinal blade axis is <100> [1,3], a natural solidification direction (*e.g.*, [4]). During high temperature service, centrifugal forces cause creep, therefore there is need for < 100 > tensile creep data. However, the solidification process not always yields precisely < 100 >-oriented crystals and deviations up to 15 ° can occur [2]. Creep anisotropy of SX is strongest in the low temperature high stress regime, where dislocation and planar fault activity on specific microscopic slip systems governs strain accumulation. In the present work we study the effect of 15 ° deviations from precise < 100 > directions combining high-resolution creep testing with micro mechanical analysis and analytical transmission electron microscopy (TEM). We investigate a SX referred to as ERBO/1 (CMSX-4 type) which was creep deformed at 1023 K and 800 MPa.

Precisely oriented miniature tensile creep samples were manufactured as described in the literature [4–7]. In the present work, we focus on three uniaxial tensile creep directions illustrated in Fig. 1. Fig. 1a shows the tensile directions in an orientation triangle. Two 15 ° deviations from the [001] loading axis (red point in Fig. 1) are considered. The green point in Fig. 1 indicates a 15 ° deviation of the tensile loading axis from [001] towards [111], while the blue point represents a deviation towards [011]. The 3D illustrations in Fig. 1b and c give a spatial impression of how the tested specimens were tilted out of the [001] crystallographic direction.

1023 K and 750 MPa creep data are presented in Fig. 2. Fig. 2a shows the tensile creep curves of the three experiments taken through to rupture in the conventional strain-time representation. In Fig. 2b, we show the same data presented as creep rates *vs.* strain in a log-linear-plot covering first 5% of deformation. Fig. 2b also contains the end points of three additional experiments (full symbols), which were interrupted after 1% strain. While there is some scatter, the data points of these interrupted tests are reasonably close to the three curves recorded in the experiments taken through to rupture.

Fig. 2 shows that the specimen with a 15 ° deviation towards [111] (green data points in Fig. 2) deforms significantly faster than the one which was misoriented towards [011] (blue data points). The specimen oriented in a precise [001] direction yields deformation rates which are in between (red data points). In SX technology material engineers must make allowances for deviations from precise [001] deviations, and 15 ° deviations have been reported to occur (*e.g.*, [2,7,8]).

As can be seen in Fig. 2, 15 ° deviations of different crystallographic nature can cause significantly different creep rates in the technologically relevant low strain range < 2%. The results obtained in the present work clearly show that 15 ° deviations from

* Corresponding author.
E-mail address: larissa.heep@rub.de (L. Heep).

https://doi.org/10.1016/j.scriptamat.2021.114274

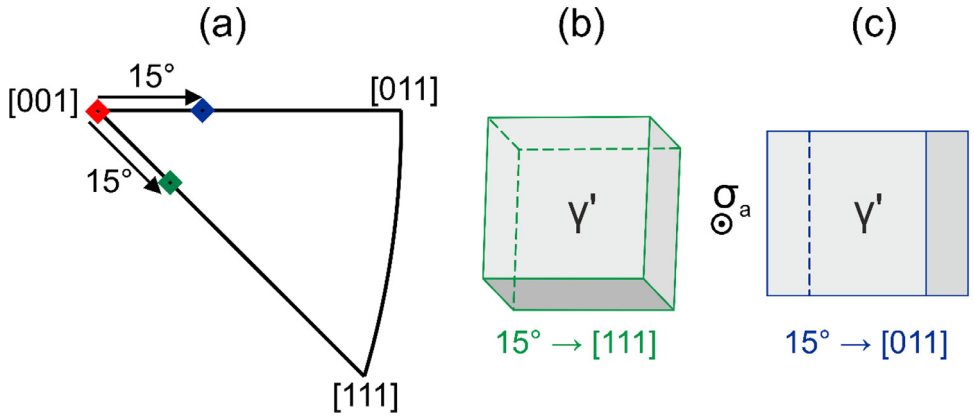

Fig. 1. Three tensile creep directions considered in the present work. (a) Orientation triangle representation. (b, c) 3D projections showing 15 ° tilts towards (b) [111] and (c) [011] (For interpretation of the references to color in this figure, the reader is referred to the web version of this article).

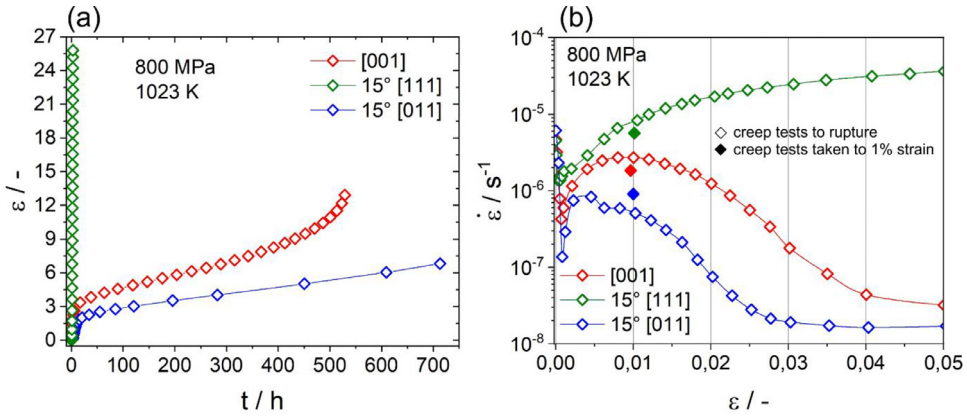

Fig. 2. Uniaxial tensile creep data for ERBO/1 (CMSX-4 type) recorded at 1023 K and 800 MPa. (a) Full creep curves presented as strain vs. time. (b) Creep data up to 5% presented as creep rate *vs.* strain in a log-linear-plot. The end points of three additional experiments are shown, which were interrupted after 1% strain (For interpretation of the references to color in this figure, the reader is referred to the web version of this article).

targeted [001] directions towards [111] show the highest creep rate.

From a fundamental point of view, a link exists between dislocation glide and climb processes and creep. Therefore, an effort was made to calculate the Peach-Köhler glide and climb forces (PK forces) normalized by the applied stress of 800 MPa and the magnitude of the Burgers vector $b = 2.49 \bullet 10^{-10}$ m, which control dislocation mobility in the three cases considered. We focus on locations in the middle of the γ-channels and in the center of γ'-particles [8]. The superposition of the applied stress σ_a and the misfit stress σ_m is considered while, in a first order approximation, the interactions with stress fields of other dislocations are neglected. Based on these stress states, PK forces F acting on dislocations with line segment directions ξ and Burgers vector b are defined as [8,9].

$$F = b \cdot (\sigma_a + \sigma_m) \times \xi \quad (1)$$

The PK glide and climb forces, F_g and F_c, are obtained as

$$F_g = (F \cdot \xi_g)\, \xi_g \text{ and } F_c = (F \cdot \xi_c)\, \xi_c \quad (2)$$

where ξ_g and ξ_c represent unit vectors in the glide and climb directions, respectively. Calculations were performed for the twelve octahedral microscopic crystallographic slip systems in the γ-channels (Numbered 1–12 in Table 1) and for the $< 112 >\{111\}$ planar fault systems [2,7] in the γ'-phase (numbered 13–24 in Table 1).

The resulting PK glide and climb force components were calculated for the three type of tensile loading conditions and the three types of γ-channels (characterized by their normal directions [001], [100] and [010]). All data are presented in Tables S1–S3 of the supplementary material.

The results summarized in Table S1 (supplementary material) indicate that [001] tensile loading results in an equal activation of 8 octahedral slip systems. Out of the full data set presented in S1, only dislocation systems 2 and 3 (reacting dislocation families) and the planar fault system 15 (containing a reaction product of the systems 2 and 3) are presented in the upper part of Table 2 (first data triple in Table 2). There are other symmetry related triples, which fulfill the same condition (see Table S1, supplementary material).

It is easy to imagine that equal activation of four planar fault systems 15, 18, 21 and 24 results in strain hardening, and it seems reasonable to assume that this is why the high symmetry [001] system shows lower creep rates at higher strains, see Fig. 2b. This is in line with what has been proposed by Yu et al. [10].

A deviation of 15 ° from [001] towards [111] results in the fastest creep rate, Fig. 2b. Here the second triple of data lines shown in Table 2 indicates that the two dislocation families, which are required for the reaction outlined by Eq. (3), have equally high resolved shear stresses and the resolved shear stress which promotes planar fault glide activity is highest. In contrast, in the case where the loading direction deviates by 15 ° from [001] towards [011], one of the reaction partners is strongly activated while the other sees a considerably lower driving force (third data triple in Table 2). This creep loading direction results in the lowest creep rates, Fig. 2b.

Table 1
Twelve microscopic crystallographic octahedral dislocation glide systems (1–12) and twelve planar fault glide systems (13–24).

Octahedral < 110 > {111} slip systems			Planar fault < 112 > {111} slip systems		
Slip system no.	Plane	Burgers vector	Slip system no.	Plane	Burgers vector
1	(111)	$[\bar{1}10]$	13	(111)	$[\bar{2}11]$
2	(111)	$[\bar{1}01]$	14	(111)	$[1\bar{2}1]$
3	(111)	$[0\bar{1}1]$	15	(111)	$[\bar{1}\bar{1}2]$
4	$(\bar{1}11)$	[110]	16	$(\bar{1}11)$	[211]
5	$(\bar{1}11)$	[101]	17	$(\bar{1}11)$	$[\bar{1}\bar{2}1]$
6	$(\bar{1}11)$	$[0\bar{1}1]$	18	$(\bar{1}11)$	$[1\bar{1}2]$
7	$(1\bar{1}1)$	[110]	19	$(1\bar{1}1)$	$[\bar{2}\bar{1}1]$
8	$(1\bar{1}1)$	$[\bar{1}01]$	20	$(1\bar{1}1)$	[121]
9	$(1\bar{1}1)$	[011]	21	$(1\bar{1}1)$	$[\bar{1}12]$
10	$(11\bar{1})$	$[1\bar{1}0]$	22	$(11\bar{1})$	$[\bar{2}1\bar{1}]$
11	$(11\bar{1})$	$[\bar{1}0\bar{1}]$	23	$(11\bar{1})$	$[1\bar{2}\bar{1}]$
12	$(11\bar{1})$	$[0\bar{1}\bar{1}]$	24	$(11\bar{1})$	$[\bar{1}\bar{1}\bar{2}]$

Table 2
Normalized Peach-Köhler force glide and climb components calculated for the three loading conditions considered. Channels are characterized by the directions, which are normal to the extension of the channel.

	Channel [001]			Channel [100]			Channel [010]		
Slip system no.	Line seg.	F_g	F_c	Line seg.	F_g	F_c	Line seg.	F_g	F_c
Precise [001] tensile loading orientation-slow (intermediate) creep rate									
2	$[\bar{1}10]$	0.633	- 0.462	$[0\bar{1}1]$	0.184	0.173	$[10\bar{1}]$	0.408	0.289
3	$[\bar{1}10]$	0.633	- 0.462	$[0\bar{1}1]$	0.408	0.289	$[10\bar{1}]$	0.184	0.173
15	$[\bar{1}10]$	0.471	- 0.717	$[0\bar{1}1]$	0.471	0.358	$[10\bar{1}]$	0.471	0.358
15 ° deviation from [001] towards [111]-fastest creep rate									
2	$[\bar{1}10]$	0.650	- 0.238	$[0\bar{1}1]$	0.201	0.061	$[10\bar{1}]$	0.426	0.177
3	$[\bar{1}10]$	0.650	- 0.238	$[0\bar{1}1]$	0.426	0.177	$[10\bar{1}]$	0.201	0.061
15	$[\bar{1}10]$	0.492	- 0.459	$[0\bar{1}1]$	0.492	0.229	$[10\bar{1}]$	0.492	0.229
15° deviation from [001] towards [011] – slowest creep rate									
2	$[\bar{1}10]$	0.707	- 0.351	$[0\bar{1}1]$	0.258	0.226	$[10\bar{1}]$	0.483	0.125
3	$[\bar{1}10]$	0.578	- 0.226	$[0\bar{1}1]$	0.354	0.250	$[10\bar{1}]$	0.129	-0.024
15	$[\bar{1}10]$	0.483	- 0.517	$[0\bar{1}1]$	0.483	0.367	$[10\bar{1}]$	0.483	0.150

Wu et al. [11] and Bürger et al. [12] have shown, that a $a/2 \cdot [\bar{1}\bar{1}2]$ ribbon required for γ'-phase cutting can form by a reaction of two ordinary γ-channel dislocations $a/2 \cdot [0\bar{1}1]$ and $a/2 \cdot [\bar{1}01]$ [11,13]. When these two γ-channel dislocation families experience similar driving forces, the probability of the reaction outlined in Eq. (3) and subsequent γ'-phase cutting increases. In the γ'-phase they create a leading super partial ($a/3 \cdot [\bar{1}\,\bar{1}2]$) and a superlattice intrinsic stacking fault (SISF). A Shockley partial segment ($a/6 \cdot [\bar{1}\,\bar{1}2]$) remains temporarily deposited in the γ-channel at the γ/γ'-interface:

$$a/2 \cdot \left[0\bar{1}1\right] + a/2 \cdot \left[\bar{1}01\right] \rightarrow a/3 \cdot \left[\bar{1}\,\bar{1}2\right] + SISF + a/6 \cdot \left[\bar{1}\,\bar{1}2\right] \quad (3)$$

Deformation substructures were studied by scanning TEM (STEM) for the material states, which were deformed to 1% strain. Thin STEM foils perpendicular to the creep loading directions were obtained by double jet electrochemical polishing in a Struers TenuPol 5. STEM investigations were performed using FEI Tecnai F20 G2 S-Twin and Jeol JEM 2100 microscopes operating at 200 kV. Large foil regions were inspected and montages (two per material state) were recorded covering projected thin foil areas larger than 150 µm² containing close to 100 γ'-particle sections each. Fig. 3 shows representative parts of the montages (which are presented in the supplementary material in Figs. S1–S3). All STEM montages were taken with $g = (200)$ with the transmitted beam parallel close to the [001] crystallographic direction. In all cases foil thicknesses were determined as described in [14]. Image analysis was used to determine the projected foil areas and the total projected fault areas. The results for the individual montages are compiled in Table S4. Average values for the three material states are listed in Table S5.

Table 3
Projected fault areas per volume A_{PF}/V in µm^{-1} for the three material states considered.

Specimen	Precise [001]	[001] → [111]	[001] → [011]
Figures	3a (part of S1)	3b (part of S2)	3c (part of S3)
A_{PF}/V in µm^{-1}	0.04	0.16	0.05

From the average results obtained from the montages in the supplementary material (Figs. S1–S3, Tables S4 and S5) projected fault areas A_{PF} per montage foil volume V were obtained which are listed in Table 3.

Even though the microstructures of Ni base SX superalloys show a high intrinsic scatter, the results presented in Figs. 3 and S1–S3 and in Table 3 allow to conclude that the material state which deforms fastest ([001] → [111]) exhibits the highest volume density of planar faults. The metallographic data do not allow to differentiate between the two material states which creep at slower rates (precise [001] and [001] → [011]).

Previous work has addressed the effect of crystallographic loading directions on creep [10,15–22]. For Mar-M200 tested at 1033 K it was reported that a creep tensile loading direction which deviated from < 100 > towards < 111 > resulted in faster creep rates than observed for precise < 100 > directions and loading directions which deviated towards < 110 > [15]. At a temperature which was only 100 K higher, this behavior changed (Mar-M200 creep tested at 1130 K): Now deviations from < 100 > towards < 111 > yield lower creep rates and it was proposed that this was due to the formation of interfacial networks, which were stabilized by dislocation reactions resulting in the formation of junctions. It was further proposed that these reactions do not occur in ten-

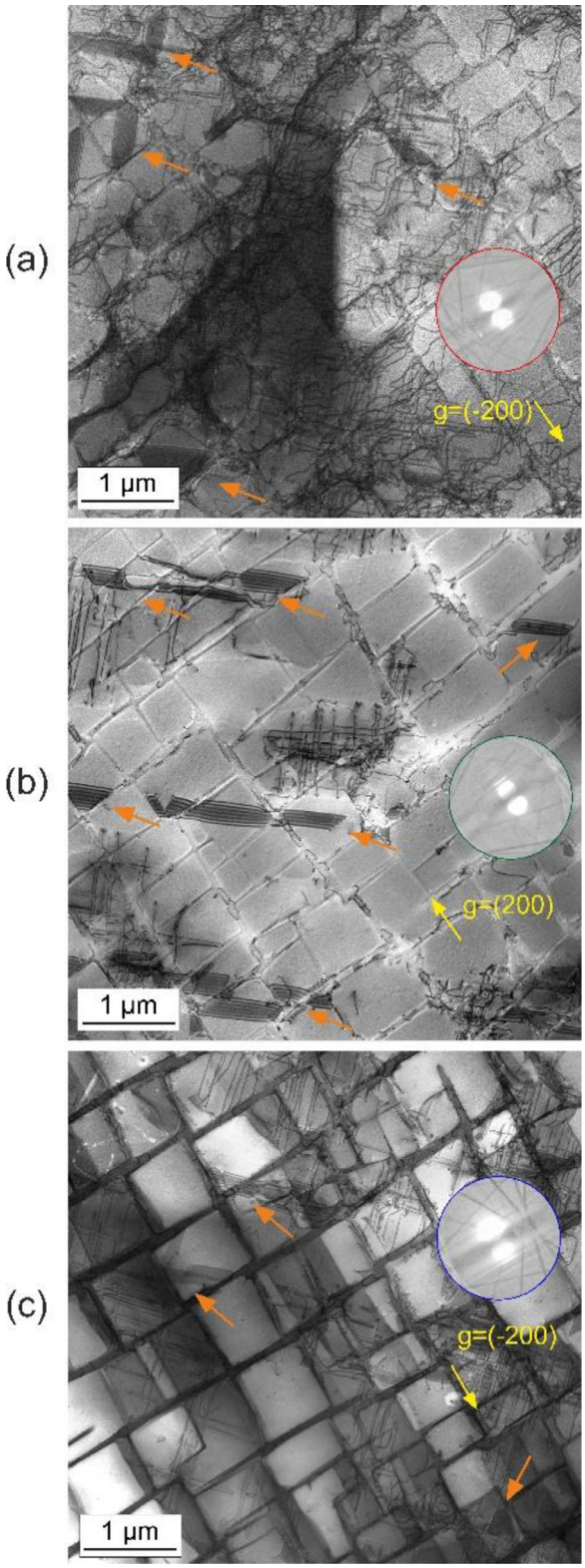

Fig. 3. Selected representative parts of full STEM montages shown in the supplementary material in Figs. S1–S3. (200) g-vectors shown as insets (diffraction spots) and as arrows. Images: (a) Precise [001] tensile loading direction. (b) 15 ° deviation from [001] towards [111]. (c) 15 ° deviation of the tensile loading direction from [001] towards [011].

sile creep specimens with loading directions which deviate from < 100 > towards < 110 > [16]. These early papers inspired many of the studies, which followed. They differed in the types of alloys which were investigated and the creep regimes which were considered [10,17–23].

Yu et al. [10] investigated a SX of type DD6 and considered deviations from the [001] direction towards [011] and [111]. In agreement to what was found in the present work, deviations towards [011] (from [001]) and precise [001] orientation showed similar low creep rates, while the specimen with a deviation from [001] towards [111] crept much faster. Yu et al. [10] present diffraction contrast TEM results showing a high density of planar faults in the γ'-phase for a crept specimen loaded in a direction, which deviated from [001] towards [111]. They attributed the corresponding high creep rate to the dominance of only one < 211 > {111} slip system. The slower creep rates for the other two directions are rationalized by a strain hardening argument, where multiple < 211 > {111} slip systems intersect.

Kakehi et al. [18] also found that orienting towards [-111]/[011] results in faster/slower creep as compared to a precise [001]-direction. They ascribed the effect of crystallographic loading directions on creep rates to different interface dislocation network configurations.

Unfortunately, the two studies [10,18] do not focus on the early stages of creep strain accumulation. Fig. 2b shows that already at the first local minimum, creep rates differ by an order of magnitude. Our explanation of the orientation effects differs from scenarios, which rely on planar fault intersections [10] and differences in interface dislocation networks [18]. While it was shown that dislocation network reactions can rationalize creep anisotropy in the high temperature low stress creep regime [24,25], different elementary deformation processes are observed at low temperatures and higher stresses [8,11]. As far as the < 112 > {111} strain hardening argument [10] is concerned, we find that up to 1% strain there are less planar faults in the creep specimen which deviated from [001] towards [011], Fig. 3.

Creep rates are governed by channel dislocation reactions, which precede γ'-cutting. This has first been suggested by Rae and co-workers, who referred to a window of opportunity [13,26–28] which opens when appropriate channel dislocation reactions occur. Wu et al. [8,11] showed how channel dislocation reactions of two dislocation families with different Burgers vectors result in the formation of the first part of a < 112 > ribbon in the γ'-phase, Eq. (3).

Clear physical evidence for the importance of equal resolved shear stresses acting on the two reacting dislocation families has been provided by Bürger et al. [12] who compared shear creep deformation of two macroscopic crystallographic shear systems < 110 > {111} and < 112 > {111} at 1023 K and a shear stress of 300 MPa. Bürger et al. [12] showed that the < 112 > shear loading direction resulted in faster creep because the two microscopic crystallographic shear systems required to fulfil Eq. (3) were both subjected to resolved shear stresses of 0.87. Note, that the activation of each of these two slip systems is less than the activation of the one which governs < 110 > {111} shear creep deformation. However, what matters is that the two slip systems, which are required to react according to Eq. (3), are equally strongly activated. Using diffraction contrast TEM, Bürger et al. [12] found that while multiple planar faults are found after 1% shear deformation in the macroscopic < 112 > {111} plane, these planar defects were absent during < 110 > {111} shear loading. It was also pointed out [8,12] that climb forces acting on the approaching octahedral dislocations make the reaction described by the Eq. (3) possible.

The present work shows, that the analysis of Bürger et al. [12] not only helps to rationalize low temperature high stress *shear* creep of superalloy single crystals. It also sheds light on the ques-

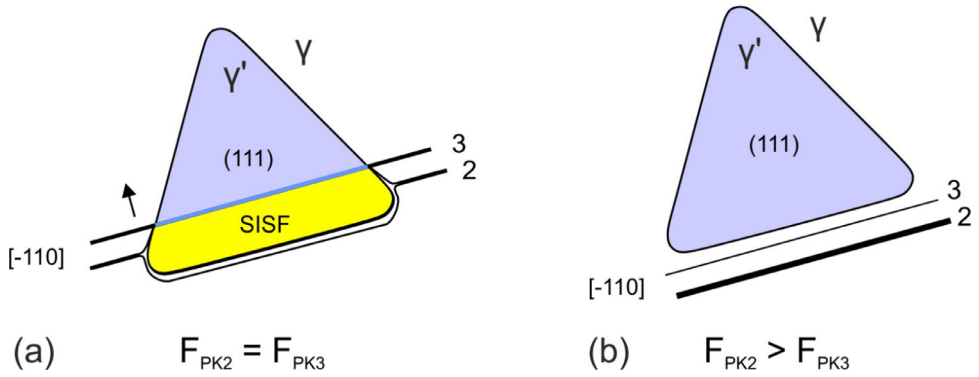

Fig. 4. Schematic illustrations of cutting / non-cutting scenarios. Dislocation families 2 and 3 from Table 2 are considered. Different resolved shear stresses are schematically illustrated by different line thicknesses. (a) Loading directions deviating by 15 ° from [001] towards [111]. (b) Loading directions deviating by 15 ° from [001] towards [011]. No cutting occurs when there is an imbalance of the intensity of activation of the two potential reaction partners (different Peach-Köhler forces represented by different thicknesses of dislocation line segments. For details, see text.

tion of whether one can accept 15 ° deviations from targeted [001] directions during *tensile* creep. The creep data presented in Fig. 2 clearly show that there is a significant difference in creep between behavior between cases where this deviation occurs towards $< 111 >$ and $< 011 >$ directions. The resolved shear stress analysis (results summarized in the supplemental material S1 to S3) in combination the creep data shown in Fig. 2 and the TEM results from Fig. 3 clearly show, that the analysis performed by Bürger et al. [12] rationalizes even the observations made in the present work where specimens were loaded in tension.

Our mechanistic interpretation shows that external resolved shear stress arguments alone are not sufficient. Instead, local stress states need to be considered including characteristic misfit stresses. The results summarized in Table 2 show that the different types of γ-channels are not equivalent in terms of PK driving forces, a fact which has been experimentally demonstrated by [29]. In further studies, an attempt must be made to incorporate dislocation-dislocation interactions, which contribute to the overall stress state [30].

Our explanation differs from what was suggested in previous studies. It underlines the importance of γ-channel dislocation reactions which precede γ'-phase cutting by planar faults. A γ' cutting process proceeding in a {111} plane is depicted in Fig. 4a. Two black lines show two dislocations in the γ-phase from dislocation families 2 and 3 listed in Table 1. Same line thicknesses reflect equal PK glide forces (see Table 2: normalized glide forces: 0.650). Fig. 4b shows a scenario, where dislocations from the same two families exhibit different Peach-Köhler glide force (represented by different line thicknesses). The normalized glide forces acting on the leading and trailing dislocations 3 and 2 are 0.578 and 0.707, Table 2.

In summary, we find that the differences in creep rates in the early stages of low temperature and high stress tensile creep between precisely oriented [001] specimens and specimens which deviate by 15 ° towards [111] and [011] directions do not rely on dislocation networks or multiple planar fault slip. Instead, they are governed by dislocation reactions between γ-channel dislocation families with different Burgers vectors, which fulfill Eq. (3). High creep rates are observed when the reacting partner dislocations are driven by similar Peach-Köhler glide forces. In the present work we successfully apply insight gained in previous work [8,11,12] to the technical issue of 15 ° deviations of cast SX from precise [001] directions and their effect on creep. The results obtained in the present work suggest that 15 ° deviations from [001] in [011] directions can be tolerated, while deviations towards the [111] direction cannot be accepted.

Declaration of Competing Interest

The authors declare that they have no known competing financial interests or personal relationships that could have appeared to influence the work reported in this paper.

Acknowledgments

LH, DB, CB, PW and GE acknowledge funding through project A2 of the collaborative research center SFB/TR 103 funded by the Deutsche Forschungsgemeinschaft DFG. AD acknowledges financial support through project ARMADIT No. CZ.02.1.01/0.0/0.0/16_025/0007304 and through infrastructural support by CEITEC within the framework of CzechNanoLab project No. LM2018110.

Supplementary materials

Supplementary material associated with this article can be found, in the online version, at doi:10.1016/j.scriptamat.2021.114274.

References

[1] M. McLean, Directionally Solidified Materials for High Temperature Service, The Metal Society, London, 1983.
[2] R.C. Reed, The Superalloys-Fundamentals and Applications, Cambridge University Press, Cambridge, 2006.
[3] T.M. Pollock, S. Tin, J. Propuls. Power 22 (2006) 361–374.
[4] K. Demtröder, G. Eggeler, J. Schreuer, Materialwissenschaft und Werkstofftechnik 46 (2015) 563–576.
[5] P. Wollgramm, D. Bürger, A. Basir Parsa, K. Neuking, G. Eggeler, Mater. High Temp. 33 (2016) 346–360.
[6] P. Wollgramm, Anisotropie des einachsigen Kriechens einkristalliner Superlegierungen im Temperaturbereich von 720°C bis 1080°C, Ruhr-Universität Bochum, 2017 Thesis.
[7] N. Matan, D.C. Cox, P. Carter, M.A. Rist, C.M.F. Rae, R.C. Reed, Acta Mater. 47 (1999) 1549–1563.
[8] X. Wu, A. Dlouhy, Y.M. Eggeler, E. Spiecker, A. Kostka, C. Somsen, G. Eggeler, Acta Mater. 144 (2018) 642–655.
[9] P.M. Anderson, J.P. Hirth, J. Lothe, Theory of Dislocations, 3rd ed., Cambridge University Press, New York, 2017.
[10] J. Yu, J.R. Li, J.Q. Zhao, M. Han, Z.X. Shi, S.Z. Liu, H.L. Yuan, Mat. Sci. Eng. A 560 (2013) 47–53.
[11] X. Wu, P. Wollgramm, C. Somsen, A. Dlouhy, A. Kostka, G. Eggeler, Acta Mater. 112 (2016) 242–260.
[12] D. Bürger, A. Dlouhy, K. Yoshimi, G. Eggeler, Crystals 10 (2020) 134 article number:.
[13] C.M.F. Rae, N. Matan, D.C. Cox, M.A. Rist, R.C. Reed, Met. Trans. A 31 (2000) 2219–2228.
[14] L.A. Jácome, G. Eggeler, A. Dlouhy, Ultramicroscopy 122 (2012) 48–59.
[15] G.R. Leverant, B.H. Kear, Metall. Trans. 1 (1970) 491–498.
[16] G.R. Leverant, B.H. Kear, J.M. Oblak, Metall. Trans. 4 (1973) 355–362.
[17] R.A. MacKay, R.D. Maier, Metall. Trans. 13 (1982) 1747–1982.

[18] K. Kakehi, T. Sakaki, J.M. Gui, Y. Misaki, in: B. Wilshire, R.W. Evans (Eds.), Proceedings of the of CFEMS, 5, Institute of Materials, London, 1993, pp. 221–230.
[19] V. Sass, W. Schneider, H. Mughrabi, Scr. Metall. Mater. 31 (1994) 885–890.
[20] V. Sass, U. Glatzel, M. Feller-Kniepmeier, Acta Mater. 44 (1996) 1967–1977.
[21] H. Murakami, T. Yamagata, H. Harada, M. Yamazaki, Mat. Sci. Eng. A 223 (1997) 54–58.
[22] V. Sass, M. Feller-Kniepmeier, Mat. Sci. Eng. A 245 (1998) 19–28.
[23] B. Koscielniak, K. Gancarczyk, M. Poreba, R. Albrecht, AMST 1 (2020) 129–134.
[24] L. Agudo Jácome, P. Nörtershäuser, J.K. Heyer, A. Lahni, J. Frenzel, A. Dlouhy, C. Somsen, G. Eggeler, Acta Mater. 61 (2013) 2926–2943.
[25] L. Agudo Jácome, P. Nörtershäuser, C. Somsen, A. Dlouhy, G. Eggeler, Acta Mater. 69 (2014) 246–264.
[26] C.M.F. Rae, N. Matan, R.C. Reed, Mat. Sci. Eng. A 300 (2001) 125–134.
[27] C.M.F. Rae, R.C. Reed, Acta Mater. 55 (2007) 1067–1081.
[28] T.M. Pollock, R.D. Field, F.N.R. Nabarro, M.S. Duesbery, in: F.N.R. Nabarro, M.S. Duesbery (Eds.), Dislocations in Solids, 11, Elsevier, Amsterdam, 2002, pp. 547–618.
[29] H.A. Kuhn, H. Biermann, T. Ungar, H. Mughrabi, Acta Mater 39 (1991) 2783–2794 Mat..
[30] M. Probst-Hein, A. Dlouhy, G. Eggeler, Mat. Sci. Eng. A 319 (2001) 379–382.